Original Article

Institution of MECHANICAL ENGINEERS
Journal of RAIL AND RAPID TRANSIT

Proc IMechE Part F:
J Rail and Rapid Transit
2023, Vol. 237(6) 751–762

DOI: 10.1177/09544097221136915
journals.sagepub.com/home/pif
Sage

Evaluating glass fiber reinforced composite sleepers to mitigate elastic fastening system spike fatigue failure: A finite element study

Christian Khachaturian[1], Marcus S Dersch[1], Shushu Liu[2] and J Riley Edwards[1]

Abstract

North American railroads have experienced spike fastener fatigue failures due to spike overloading that have led to multiple derailments. Failures have primarily been found in timber sleeper track constructed with elastic fasteners. This is likely because the elastic fasteners change the load path, resulting in spikes becoming a primary component to transfer the longitudinal forces. Mitigation methods to prevent spike overloading have been limited and thus, this novel study seeks an alternative method leveraging engineered composite sleepers to reduce spike stress. This paper first documents and compares typical composite and timber sleeper properties as reported in the literature. Then, this paper describes the development and validation of a single spike-in-sleeper finite element model (FEM) used to investigate the interaction between the composite sleeper and spike. A glass fiber reinforced composite (GFRC) sleeper was selected due to its high elastic modulus and compressive strength reported in the literature. The validated model was used to quantify the effect of these critical material properties on spikes subjected to longitudinal loads. The GFRC's stiffness and compressive strength values lead to a 30% reduction in the maximum spike stress when compared to spikes installed in timber sleepers. The reduced spike stress in the GFRC fell below the spike's expected fatigue limit. Finally, this paper provides required compressive strength for given longitudinal loads to ensure the spike stress falls below the fatigue limit in different operating environments. This characterization of required composite sleeper strength properties can be used to advance track system mechanistic-empirical design.

Keywords

spike fatigue failure, composite sleepers, laboratory experimentation, finite element analysis, finite element model, sleeper compressive strength

Date received: 29 April 2022; accepted: 18 October 2022

Introduction

Over the past 20 years there have been at least twelve derailments on four different railroads in the United States as a result of fatigue-failed spikes in timber sleepers.[1] The location of spike failure usually occurs 38.1 mm (1.5 in) below the top of sleeper, which makes detection of failed spikes both time and labor intensive as it requires manual walking inspection.[2] Several research studies have been conducted to determine the root cause of these broken spikes in the elastic fastening systems with timber sleepers.[3–6] It was found that spike fatigue failures occur most commonly in timber sleeper tracks constructed with elastic fastening systems. These elastic fasteners change the load path and increase the longitudinal demand placed on the spike due to (1) lack of anchor;[1] (2) loss of friction at the plate-sleeper interface due to rail uplift;[6,7] and (3) higher stiffness.[6] Therefore, locations most likely to experience spike overloading fatigue failures include higher degree curves, special trackwork, steep grades and other locations subjected to high longitudinal and lateral loads, tractive effort, and braking forces as these are the most common locations elastic fasteners would be installed to prevent rail-rollover derailments.[8] Several methods to eliminate the failures have been proposed. These mitigation methods have primarily focused on fastening system design[1,4] as well as operational and maintenance activities.[9] However, most of the mitigation methods have, thus far, only delayed the spike failure. Therefore, a mitigation method that can prevent spikes from fatigue failure and hence significantly improve the longevity of spike is desired.

In the United States, over 90 percent of Class I railroad track miles utilize timber sleepers. Timber sleepers can be characterized as an orthotropic material given their properties vary in each direction. Timber has a greater modulus of elasticity and higher strength parallel to grain

[1]Rail Transportation and Engineering Center—RailTEC, Department of Civil and Environmental Engineering—CEE, Grainger College of Engineering—GCoE, University of Illinois at Urbana-Champaign—UIUC, Urbana, IL, USA
[2]Changeis Inc. Volpe National Transportation Systems, Cambridge, MA, USA

Corresponding author:
Corresponding author: Shushu Liu, Changeis Inc., Volpe National Transportation Systems Center, 55 Broadway, Cambridge MA 02142, USA.
Email: shushu.liu.ctr@dot.gov

than those perpendicular to grain direction.[10] When longitudinal loads are transferred to timber sleepers, the loads crush the timber fibers more easily due to the weaker strength in the perpendicular to grain direction. As a result, timber sleepers deteriorate faster when subjected to longitudinal loads, which further increases the spike stress and accelerates its failure.[11] While prestressed concrete and steel sleepers have been used in the past decades, the increased depth of concrete, low-impact resistance, high weight, and cracking are serious problems.[12] Additionally, risk of corrosion, electrical conductivity, fatigue cracking and difficulty of installation are the major limitations of steel sleepers.[13] Given these challenges, composite sleepers have emerged as an alternative to timber sleepers.[14] Many composite sleepers are composed of post-consumer recycled plastic while others use virgin polymers. Additives, fillers, and fiber or particle reinforcement may be used to enhance specific properties.[15] Unlike timber, the composite sleepers do not require preventative treatment and are impervious to rotting and insect infestation and thus perform at a comparable level to timber sleepers but last longer.[16] As an engineered product, composite sleepers are isotropic with high modulus of elasticity and compressive strength in all directions. Although the modulus of elasticity and compressive strengths of the composites are not always higher than those of the timber parallel to grain direction, the composites provide an opportunity to improve the sleeper's performance when loaded longitudinally (i.e. the direction perpendicular to grain where timber's modulus of elasticity and compressive strengths are much weaker). A variety of research studies have been conducted on composite sleepers. However, the research has mainly focused on the failure modes,[17–18] thermal effect,[16] and mechanical behavior under various loading conditions.[19,20] Information on investigating load transfer to other components, such as spike stress distribution, in composites was unavailable.

This paper investigates the feasibility of using composite sleepers as a remediation method to reduce spike stress. The following sections document the typical composite sleeper properties as reported in the literature, compared composites to timber sleepers, and then document the development, validation, and use of a single spike-in-sleeper finite element model (FEM) to characterize the interaction between the composite sleeper and spike.

Composite and timber sleeper comparison

A comprehensive literature review was conducted to compare material properties of each composite sleeper on the market.[21–28] The modulus of elasticity (MOE) (Figure 1, top) and compressive strengths (Figure 1, bottom) for timber and composite sleepers are summarized below (Figure 1). Among the composite sleepers, a novel glass fiber reinforced composite (GFRC) sleepers provide a skin with higher MOE and compressive strength than other composites. The GFRC is constructed with glass fiber-reinforced 100% recycled polyolefin plastic and consists of a 0.5∼1.0 in. fiber-reinforced outer layer (i.e. skin), surrounding an inner core which is constructed with lower strength materials.

Figure 1 shows that the compressive strength of composites ranging from 6.2–45.5 MPa (900–6600 psi). Although these values vary significantly, the weakest composite compressive strength (6.2 MPa (900 psi)) is 34% greater than the strongest timber perpendicular-to-grain compressive strength (4.4 MPa (639 psi)). Composite MOE ranges from 730.8–2920 MPa (106,000–424,000 psi) which is comparable to the timber perpendicular-to-grain range of 482–1720 MPa (70,000–250,000 psi). However, the strongest non-GFRC composite MOE (2920 MPa (424,000 psi)) is 49% lower than the weakest timber parallel-to-grain MOE (4830 MPa (700,000 psi)). The median MOE of composites was 43% greater than the median of timber-perpendicular-to-grain but 146% lower than timber parallel-to-grain. The median composite compressive strength is 150% greater than the median of the timber perpendicular-to-grain, while again, composite values are 35% lower than timber parallel-to-grain. Among the composite sleepers found in the literature, the GFRC provides a compressive strength superior to timber (parallel-to-grain and perpendicular-to-grain), and an MOE that is superior to timber perpendicular-to-grain, but still lower than timber parallel-to-grain.

Due to the novelty of the GFRC, few feasibility studies are available in the literature. While previous studies have focused on the sleeper performance,[29,30] and its influence on the track substructure,[14, 31] this study investigates the effect of the GFRC composite sleeper on spike stress.

Model development

A previously developed single-spike FEM previously developed was modified and used in this study.[11] This FEM was originally developed to quantify the spike and timber sleeper response when subjected to various loading conditions. For this study, the FEM was modified to represent a fiber reinforced composite sleeper with a 0.75-in thick "skin" and remaining "core." The model consisted of a single spike embedded in a block (457 mm (18 in.) × 178 mm (7 in.) × 229 mm (9 in.)) representing the section of a sleeper (Figure 2). Typically, unrealistic stress concentration would develop on the spike when loads were directed applied on the spike surface. To avoid the artificial local stress concentration, portions of a rail plate were modeled around the upper shaft of the spike and the longitudinal force (F_{long}), was as applied on the plate. This approach simulated the load path transferred from the plate to the spike, and hence avoided applying concentrated forces directly to the spike.

The element sizes for the spike and plate were 0.1 inches, and mesh sizes for the sleeper were 0.4 inches. These element sizes were considered appropriate for eliminating mesh sensitivity concerns while balancing the demands on computational resources. A mesh sensitivity analysis was accomplished by comparing the maximum von Mises stress values on the spike with different spike mesh sizes. Four mesh sizes of spike were generated for the analysis: 0.4 inches, 0.2 inches, 0.1 inches and 0.05 inches (Figure 3). As the mesh sizes became smaller, the von Mises stress on the

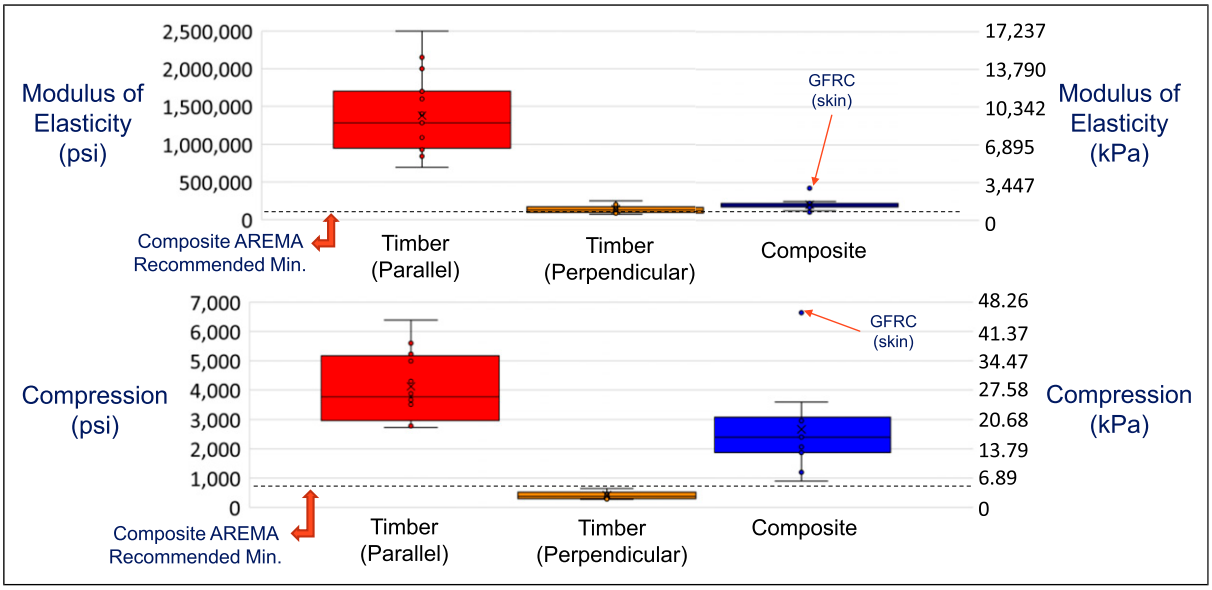

Figure 1. Composite and timber modulus of elasticity (top) and compressive strength (bottom) properties.

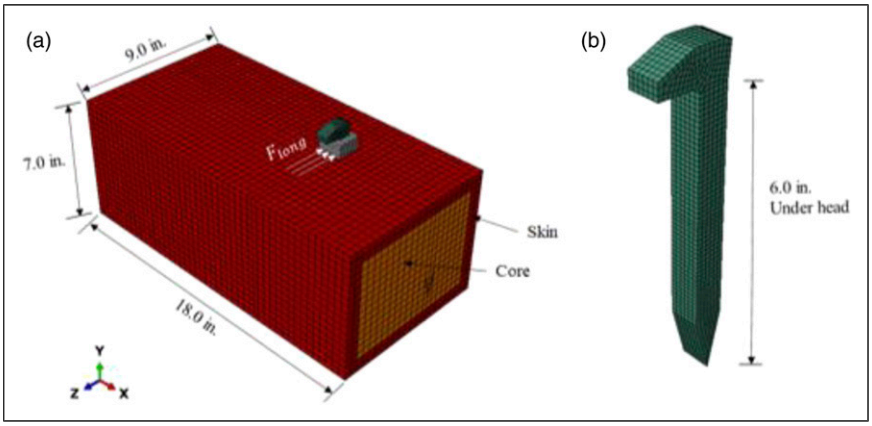

Figure 2. Single spike-sleeper FEM with dimensions, mesh, and location of load application (a) and detailed meshed spike (b).

spike increased initially, and the value then experienced minimal change (i.e. only 1.6% increase from mesh sizes 0.1 inches to 0.05 inches), indicating the results were no longer sensitive to the mesh sizes. Therefore, a mesh size of 0.1 inches was selected for the spike. All of the components were modeled as 3D deformable solids, meshed using linear brick, element type C3D8. A total of 2766 elements were generated for the spike, 7008 elements for the plate and 19,454 elements for the sleeper. The coefficient of friction between the steel spike and the sleeper was defined to be 0.3. The model was designed to examine the responses of the steel spike and sleeper to loads applied directly on the upper shaft of the spike through the plate. A frictionless interaction was assigned between the plate and sleeper such that 100% of the longitudinal load was transmitted to the spike. In the model, the bottom and the long sides of the sleeper were fixed from translation and rotation to be consistent with the laboratory test setup.

Definitions of spike steel material properties used are comparable to AISI 1022, 1025, or 1030 steel with a Young's modulus of 213,000 MPa (30,850 ksi) and Poisson's ratio of 0.3. The spike has typical ultimate tensile strengths ranging from 0.51–0.83 MPa (74 - 120 ksi). In this study, an ultimate tensile strength of 586 MPa (85 ksi) and a corresponding yield strength of 386 MPa (56 ksi) were assigned to the steel spike material as quantified by Dersch et al.[3] The fatigue endurance limits of steel are typically estimated to be half of the ultimate tensile strengths, and thus for the material modeled, would be 296 MPa (43 ksi), which is also 76% of the yield strength. The spike would experience fatigue failure upon repetitive loads once the spike stress exceeds the fatigue limit, therefore, as a rule of thumb in the design, it is desirable to control the spike stress below the fatigue limit.

Elastic properties are not adequate to model the sleeper behavior as the sleeper would experience damage as excessive loads are transferred from the spike, and in turn, increase the maximum spike stress.[11] After a search of the Abaqus documentation,[32] a user material (UMAT) subroutine with damage criterion was used to simulate the behavior of the sleeper. This UMAT model used two damage variables to describe the damage in the fiber and matrix, respectively. Required inputs for the UMAT model include the elastic properties, strength limits governing

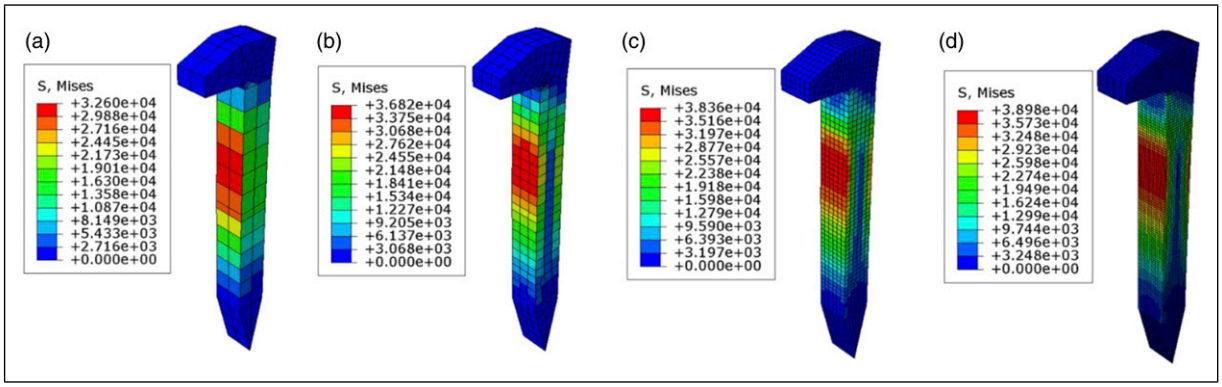

Figure 3. Mesh sensitivity analysis on spike with mesh size: (a) 0.4 in; (b) 0.2 in; (c) 0.1 in; and (d) 0.05 in.

damage initiation, and fracture energy prescriptions governing damage evolution. In the UMAT model, damage in the fiber direction f_f is initiated when the following criterion is reached:

$$f_f = \sqrt{\frac{\epsilon_{11}^t}{\epsilon_{11}^c}(\epsilon_{11})^2 + \left(\epsilon_{11}^t - \frac{(\epsilon_{11}^t)^2}{\epsilon_{11}^c}\right)\epsilon_{11}} > \epsilon_{11}^t \qquad (1)$$

where, ϵ_{11}^t and ϵ_{11}^c are the failure strains in fiber direction in tension and compression, respectively. Failure occurs when f_f exceeds its threshold value ϵ_{11}^t.

Once the above criterion is satisfied, the fiber damage variable, d_f, evolves according to the equation

$$d_f = 1 - \frac{\epsilon_{11}^t}{f_f} e^{\left(-C_{11}\epsilon_{11}^t\left(f_f - \epsilon_{11}^t\right)/G_f\right)} \qquad (2)$$

where G_f is specific fracture energy. C_{11} is the component of elasticity matrix along fiber direction in the undamaged state. Similarly, damage initiation in the matrix f_m is governed by the criterion

$$f_m = \sqrt{\frac{\epsilon_{22}^t}{\epsilon_{22}^c}(\epsilon_{22})^2 + \left(\epsilon_{22}^t - \frac{(\epsilon_{22}^t)^2}{\epsilon_{22}^c}\right)\epsilon_{22} + \left(\frac{\epsilon_{22}^t}{\epsilon_{12}^s}\right)^2(\epsilon_{12})^2} > \epsilon_{22}^t \qquad (3)$$

where ϵ_{22}^t and ϵ_{22}^c are the failure strains perpendicular to the fiber direction in tension and compression, respectively. The failure strain for shear is ϵ_{12}^s. Failure occurs when f_m exceeds its threshold value ϵ_{22}^t.

The evolution law of the matrix damage variable, d_m, is

$$d_m = 1 - \frac{\epsilon_{22}^t}{f_m} e^{\left(-C_{22}\epsilon_{22}^t\left(f_m - \epsilon_{22}^t\right)L^c/G_m\right)} \qquad (4)$$

where C_{22} is the component of elasticity matrix perpendicular to the fiber direction in the undamaged state.

During progressive damage the effective elasticity matrix is reduced by the two damage variables d_f and d_m, as follows:

$$C_d = \begin{bmatrix} (1-d_f)C_{11} & (1-d_f)(1-d_m)C_{12} & (1-d_f)C_{13} & 0 & 0 & 0 \\ 0 & (1-d_m)C_{22} & (1-d_m)C_{23} & 0 & 0 & 0 \\ 0 & 0 & C_{33} & 0 & 0 & 0 \\ & & & (1-d_f)(1-d_m)C_{44} & 0 & 0 \\ & \textit{symmetric} & & 0 & C_{55} & 0 \\ & & & 0 & 0 & C_{66} \end{bmatrix} \qquad (5)$$

where C_{ij} are the components of elasticity matrix in the undamaged state.

A recent field investigation[5] on a heavy axle load (HAL) freight and passenger corridor reported the 99th , 95th, and 90th percentile longitudinal spike loads to be 8.9 kN (2000 lbf), 7.7 kN (1700 lbf), 6.7 kN (1500 lbf), respectively, assuming that a single spike was subjected to 70% of the applied rail seat load.[4,33] Therefore, the maximum load, 8.9 kN (2000 lbf) was applied to the spikes in this study.

Model validation

The properties of the sleeper in the FEM were calibrated and compared to laboratory test results. The laboratory test consisted of applying a load to an instrumented spike that was installed in a GFRC sleeper (Figure 4(a)). The sleeper block was 457 mm (18 in.) long × 178 mm (7 in.) wide × 229 mm (9 in.) high and was restrained to prevent translation and rotation of the two sides of the sleeper. The loading fixture that represented the rail plate was approximately 1.27 mm (0.05 in.) above the top surface of the sleeper to eliminate friction and align with the model assumptions. A novel instrumented spike (Figure 4(b)) as

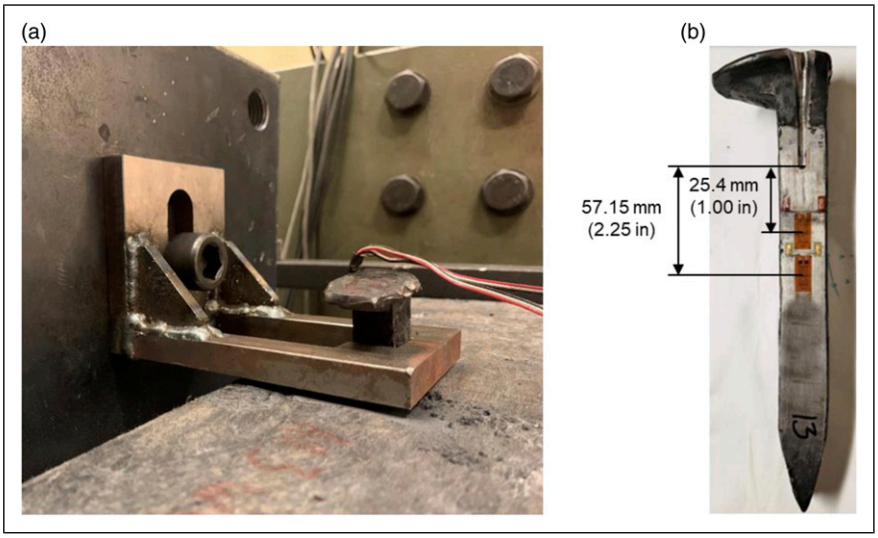

Figure 4. Instrumented spike installed in the sleeper (a) and layout of strain gauges used for FEM calibration (b).

(a)

		Modulus of Elasticity MPa (psi)	Compression MPa (psi)	Tension MPa (psi)
Test	Skin	3,503 (508,000)	45.5 (6,600)	37.9 (5,500)
	Core	1,179 (171,000)	20.7 (3,000)	27.6 (4,000)
Model	Skin	3,434 (498,000)	41.4 (6,000)	34.5 (5,000)
	Core	2,000 (290,000)	20.7 (3,000)	8.3 (1,200)

(b)

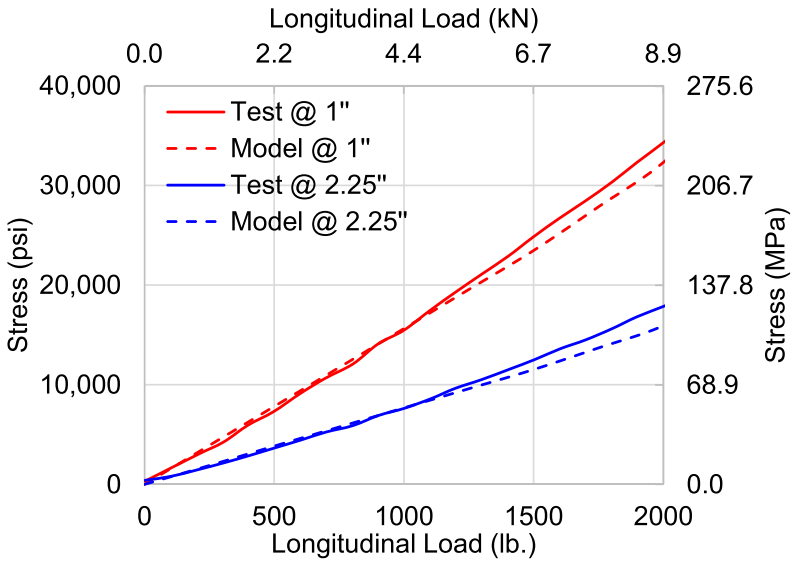

Figure 5. Model validation: (a) Composite sleeper laboratory material property laboratory test results and calibrated model values; and (b) Comparison between laboratory recorded and FEM output spike stress.

documented by Dersch et al.[4] was used to measure the spike bending stress during the loading. The spike consisted of two strain gauges, which when installed, were located at 25.4 mm (1.0 in.) and 57.15 mm (2.25 in.) below the top sleeper surface. The strain gauges were attached directly on the prepared surface of the spike so that they did not change the behavior of the system. Epoxy was used to protect the wires and strain gauges during spike insertion and loading. The instrumented spike was driven into a composite sleeper and an 8.9 kN (2000 lb.) longitudinal load was applied through the loading fixture.

In the FEM, the elastic modulus and strength properties of the sleeper were varied until the spike stress at 25.4 mm (1 in.) and 57.15 mm (2.25 in.) below the sleeper surface matched the laboratory measurements. The properties of the calibrated composite sleeper FEM were found to be

representative of the GFRC materials tested in the laboratory (Figure 5(a)) when adjusting for expected manufacturing variability.

The spike stress quantified with the laboratory test and model output at the strain gauge locations were compared (Figure 5(b)). At both locations, the spike stress increased with the applied longitudinal load, as expected. Further, the FEM had excellent agreement with the test results, suggesting that the parameters used in the FEM were appropriate, thus validating the FEM.

Results & discussion

As shown in Figure 5(a), the skin of GFRC provides a modulus of elasticity 1.7 times larger than the core, and its compressive strength is twice as large as the core. To understand the role of the reinforced skin plays in spike stress distribution, two scenarios, as presented in Figure 6(a), were investigated in the model: Case 1 represents the GFRC that contains the skin and core with the calibrated parameters; and Case 2 is an unreinforced homogeneous sleeper that the properties of the skin region are assumed to be the same as the core. Comparing the two cases, the core regions have the same material properties, but the skin region in Case 1 is stiffer with a stronger compressive strength.

The bending deformation of the spike when an 8.9 kN (2000 lb.) longitudinal load was applied for both cases was compared (Figure 6(b)). Prior to the loading, the spike was in a neutral position with zero deformation along the depth. When the longitudinal load was applied, the top region of the spike in contact with the sleeper surface initiated the bending deformation first, and the bending deformation gradually extended to the entire spike shaft. The homogenous sleeper in Case 2 exhibited approximately 30% larger deformation than the spike in the composite sleeper (Case 1) due to it being softer and weaker.

Different bending deformation resulted in different spike stress distributions for the two cases (Figure 6(c)). Generally, the larger bending deformation in Case 2 resulted in 20% more stress on the spike. In Case 1, the maximum spike stress was approximately 276 MPa (40 psi), falling below the fatigue limit, 296 MPa (43 ksi); while in Case 2, the maximum spike stress was approximately 331 MPa (48 psi), exceeding the spike fatigue limit. This indicates the potential of spike fatigue failure when subjected to repeated load applications.

The smaller deformation and lower spike stress in Case 1 is partially a result of the increased compressive strength of the skin, as higher strength materials would not fail and thus would reduce the amount of spike bending. Therefore, to further investigate the effect of skin compressive strength, parameters in Case 2 were used as a baseline and the compressive strength of the skin was varied from 20.7 MPa (3000 psi) to 41.4 MPa (6000 psi). The spike stresses with different skin compressive strengths were recorded and compared to the spike fatigue limit (Figure 7).

The spike stress decreased as the skin compressive strength increased. When the compressive strength was below 34.5 MPa (5000 psi), the spike stress was above the fatigue limit, suggesting the spike would experience fatigue failure under repeated load applications. As compressive strength increased, there was a decreasing benefit on spike stress reduction. When the compressive strength was above 34.5 MPa (5000 psi), the spike stress was below the fatigue limit and had little variations with additional compressive strength gains. Therefore, there was minimal value in increasing the compressive strength beyond the compressive strength of 34.5 MPa (5000 psi), when only considering the application of longitudinal loads. This suggests that spike stress is not sensitive to sleeper compressive strength if the sleeper provides sufficient strength against the load. The results presented in Figure 7 are also consistent with Yu et al.[34] that compressive stress of the sleeper was found to dominate the

(a)

	Modulus of Elasticity (MPa/psi)	Compression (MPa/psi)	Tension (MPa/psi)	Shear (MPa/psi)
Case 1: Skin	3,434/498,000	41.4/6,000	34.5/5,000	4.1/600
Case 1: Core	2,000/290,000	20.7/3,000	8.3/1,200	4.1/600
Case 2: Skin	2,000/290,000	20.7/3,000	8.3/1,200	4.1/600
Case 2: Core	2,000/290,000	20.7/3,000	8.3/1,200	4.1/600

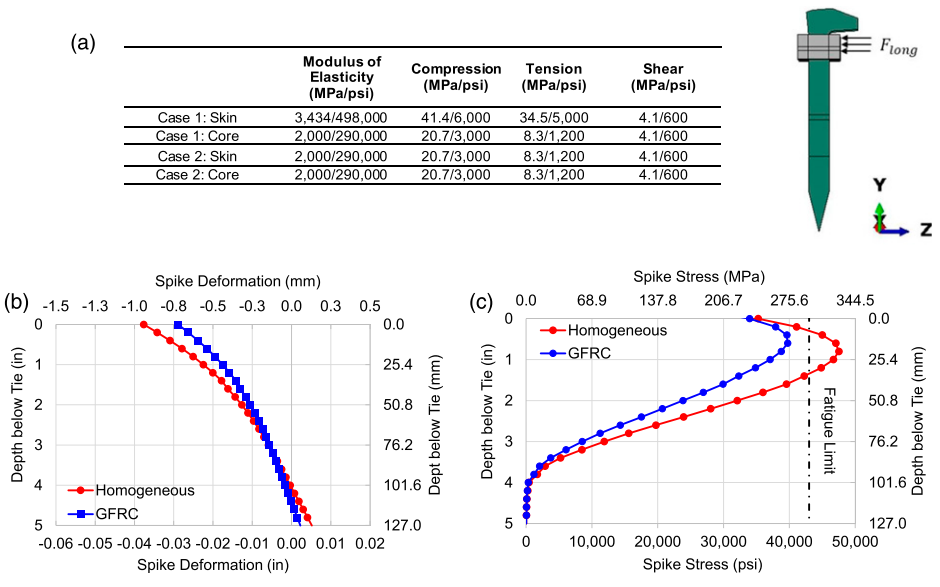

Figure 6. Comparison between GFRC and homogeneous sleeper: (a) material properties of case study; (b) spike deformation when subjected to an 8.9 kN (2000 lb.) longitudinal load; and (c) Spike stress distribution with depth.

spike bending behavior and consequently affected the spike stress. In addition to the compressive stress, Yu et al.[34] concluded that the spike behavior was also affected by the shear stress of the sleeper, which was not observed through the parametric study in this paper. It is likely due to the magnitude of the applied load. In this study, a 2000 lb. of longitudinal load was applied on the spike, which presents a realistic heavy-haul loading environment but the magnitude is smaller than that in Yu et al.[34] It is believed that the shear failure would occur if the longitudinal load continued to increase. Research studies are recommended to further investigate this subject when the heavy haul loading environment becomes severer.

Next, to investigate the effect of MOE on spike stress, the properties of the skin were varied from (2000 MPa (290,000 psi) to 3434 MPa (498,000 psi)), and the spike stress was recorded (Figure 8). For this study, sleeper compressive strength was held constant at 41.4 MPa (6000 psi), to ensure the sleeper provided sufficient strength to prevent compressive failure.

The results indicate an inverse relationship between sleeper MOE and the maximum spike stress. That is, as modulus increased, maximum spike stress decreased. This is a result of reduced spike bending due to greater confinement, which aligns with previous findings by Dersch et al.[3] Although an inverse relationship between elastic modulus and spike stress was confirmed, the stress reduction was marginal (approximately 4%). This is likely a result of the current range of elastic modulus values. When considering the maximum feasible elastic modulus for a composite sleeper, the magnitude is still less than 50% of a timber sleeper. Figures 7 and 8 indicate that compressive

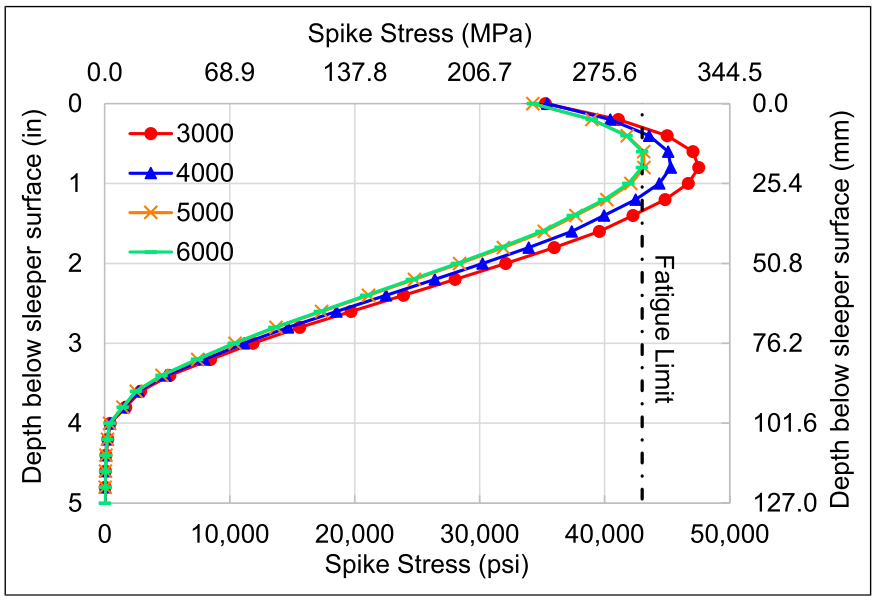

Figure 7. Effect of sleeper compressive strength on spike stress.

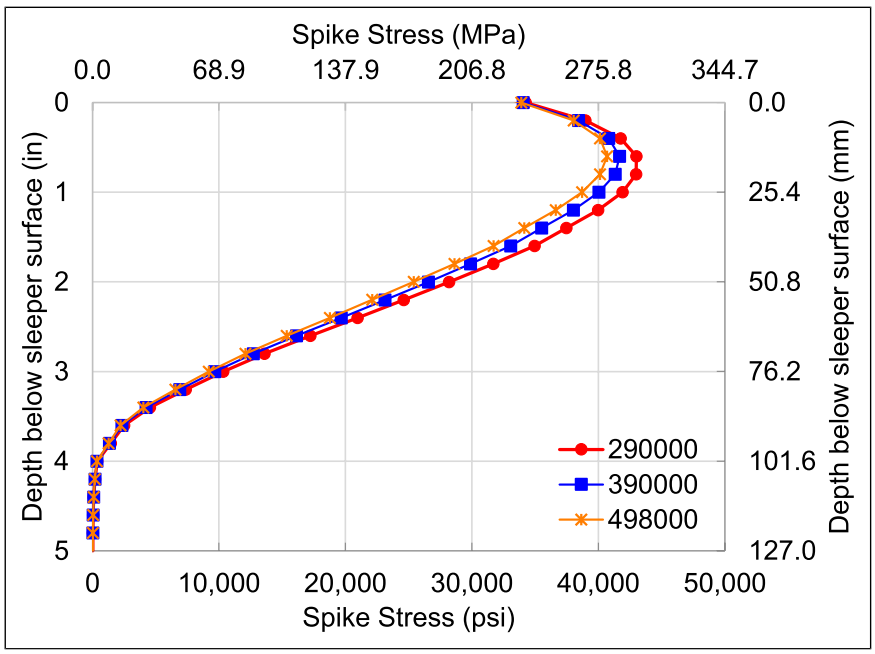

Figure 8. Effect of MOE on spike stress.

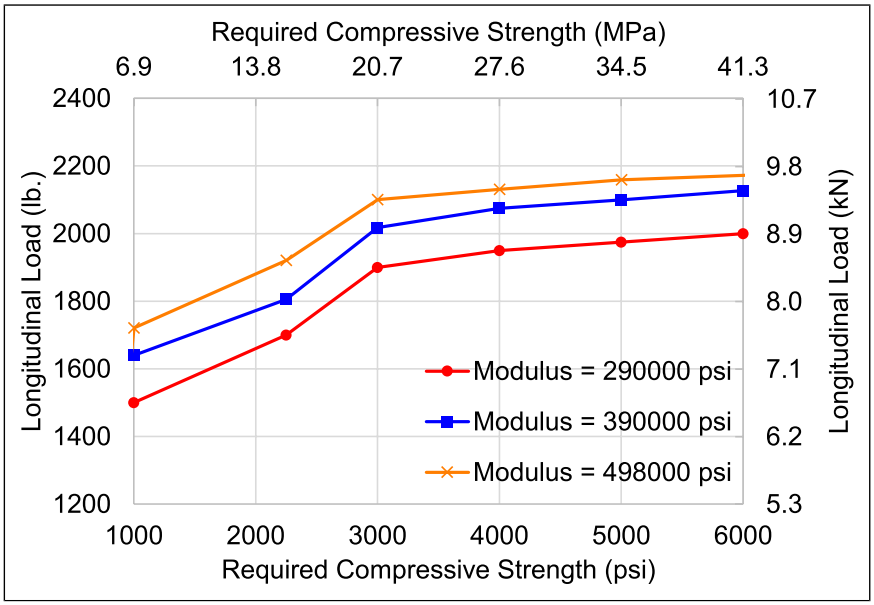

Figure 9. Compressive strength of composite sleeper to reduce spike stress below fatigue limit.

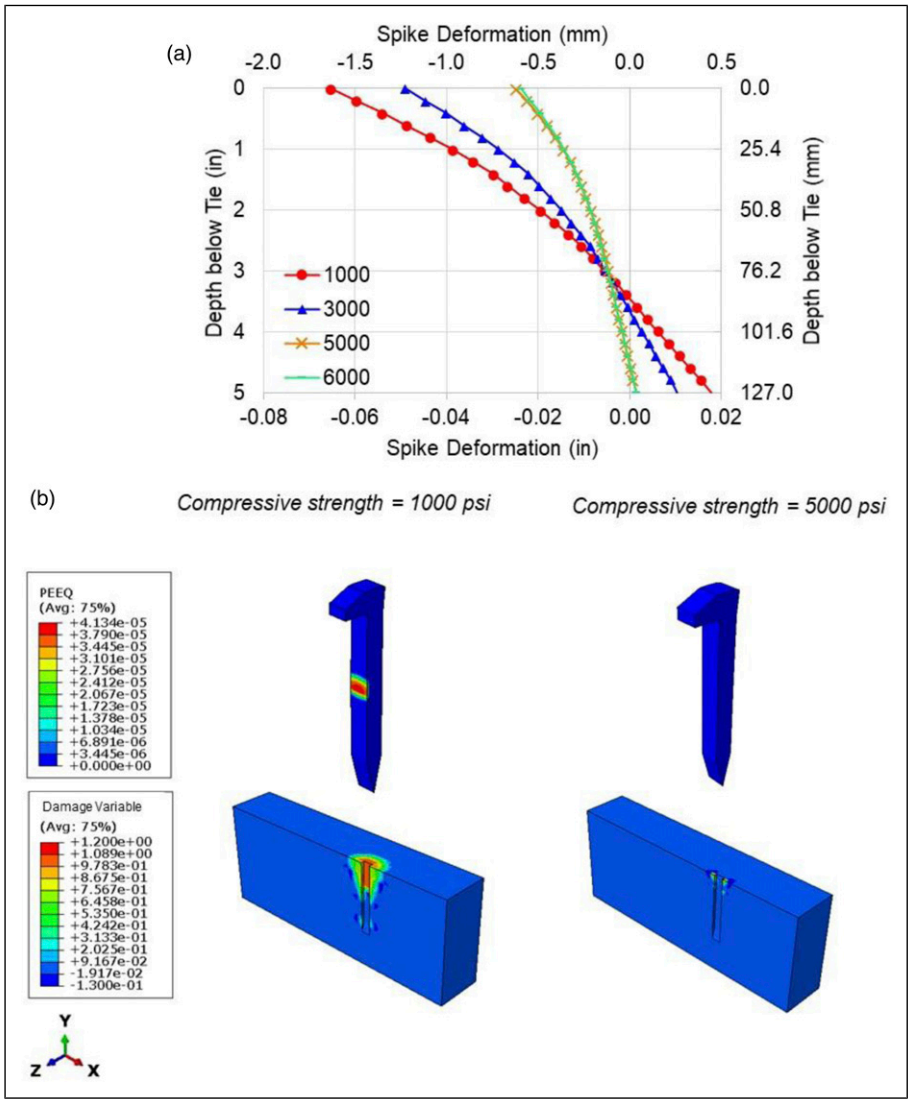

Figure 10. Effect of compressive strength on: (a) spike deformation; and (b) Typical spike plastic deformation and sleeper damage.

(a)

Parallel to Grain (L)			Perpendicular to Grain (T)			
Modulus of Elasticity MPa (psi)	Compressive Strength MPa (psi)	Tensile Strength MPa (psi)	Modulus of Elasticity MPa (psi)	Compressive Strength MPa (psi)	Tensile Strength MPa (psi)	Longitudinal Shear Strength MPa (psi)
11,376 (1,650,000)	20.7 (3,000)	49.4 (7,161)	1,338 (194,000)	1.62 (235)	1.86 (270)	5.52 (800)

(b)

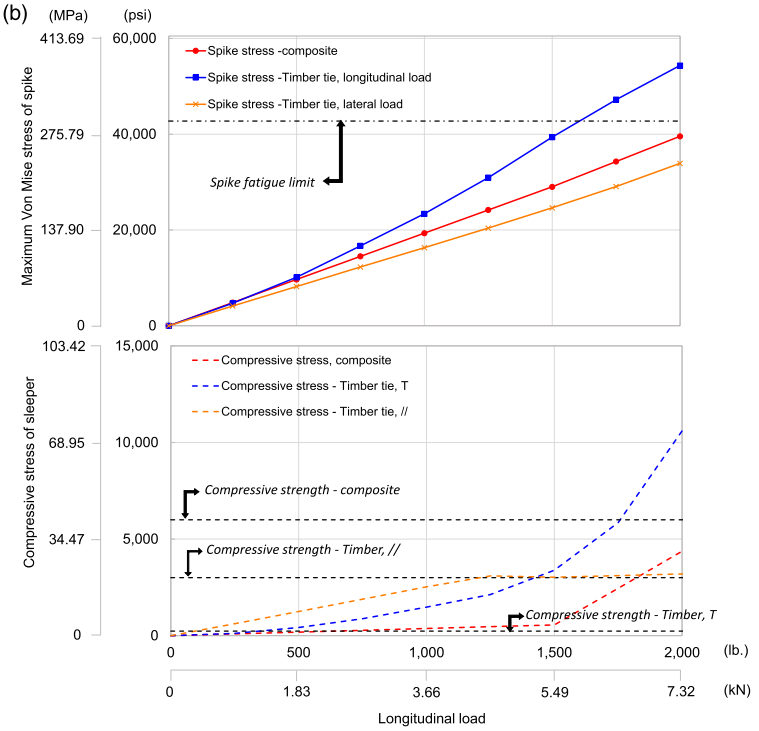

Figure 11. Comparison between GFRC and timber sleeper: (a) properties of timber sleeper; and (b) spike stress and sleeper compressive stress with load.

strength has a more significant effect on spike stress reduction compared to elastic modulus as it relates to engineered composite sleepers for the maximum expected loads. This aligns with the findings of Dersch et al.[3] which found that compressive strength has a greater effect than modulus of elasticity on spike stress.

To identify the required compressive strength thresholds for lower longitudinal loads, an additional parametric study was performed varying MOE and the load applied (Figure 9).

As previously discussed, for a given compressive strength, a larger modulus decreased the spike stress, therefore, the threshold to ensure the spike stress below the fatigue limit increased. For a given modulus of elasticity, as compressive strength increased the sleeper was able to carry increased longitudinal loads. For example, with modulus of 2000 MPa (290,000 psi), to reduce spike stress below the fatigue limit for a 95th percentile longitudinal spike load of 7.6 kN (1700 lb.),[5] a compressive strength of 15.34 MPa (2225 psi) is required. Comparatively, considering a 90th percentile longitudinal spike load of 6.7 kN (1500 lb.),[5] a compressive strength of 6.89 MPa (1000 psi) is required. Therefore, all composite sleepers found in the literature would exhibit an adequate compressive strength to withstand the 90th percentile load and most would withstand a 95th percentile load.

As the compressive strength continued to increase, the threshold for the longitudinal load tended to stablize, likely because the compressive failure would not be a dominant failure mode for the sleeper. If the longitudinal load exceeded 8.9 kN (2000 lb.), shear failure of the spike could be expected. Therefore, in these instances, an alternative sleeper design would not be a solution to the fatigue-failed spike problem. Although the effect of a uni-directional longitudinal load is quantified (Figure 9), more research is needed to quantify the impact of simultaneously applied lateral and longitudinal loads on the required sleeper's compressive strength to reduce spike stress below the fatigue limit. As is the case if longitudinal loads exceed 8.9 kN (2000 lb.), and/or if the combination of lateral and longitudinal loads exceeds a specific resultant load, composite sleepers might delay spike failure, but would not be expected to eliminate it.

To visualize the effect of increasing sleeper compressive strength, the spike permanent deformation (equivalent plastic strain parameter, defined as PEEQ in ABAQUS) and timber damage are presented (Figure 10).

It can be seen that the spike had larger deformation in the sleeper with weaker compressive strength, resulting in greater spike bending stresses, as discussed previously. When the compressive strength of the sleeper was 6.9 MPa (1000 psi), the spike had the largest deformation, leading to the largest bending stress on the spike. Further, when the compressive strength of the sleeper reached the minimum required strength (above 34.5 MPa (5000 psi) in Figure 10(a)), the deformation of the spike was no longer affected by further increases in sleeper compressive strength.

In the model, once the von Mises stress reaches the yield strength, irreversible permanent plastic deformation is developed leading to nonnegative equivalent plastic strain parameter, PEEQ, to become greater than zero, indicating damage initiation of the component. When the composite sleeper compressive strength was 34.5 MPa (5000 psi), the maximum von Mises stress of the spike was below the yield strength, 586 MPa (56 ksi), and thus there was no plastic deformation on the spike, suggesting an elastic state of the spike. Additionally, for this case, there was minimal damage of the timber. However, when the composite sleeper compressive strength was 6.9 MPa (1000 psi), the maximum von Mises stress of the spike exceeded the yield strength, and thus, a non-zero value of PEEQ was shown on the spike, suggesting irreversible plastic deformation. Further, for this case, the sleeper shows significant damage which would likely lead to additional deformations with cyclic loads and failed spikes in the field.

Finally, unlike most composites, timber sleepers are orthotropic with strength properties parallel to grain being approximately 10-times stronger than perpendicular to grain. When timber sleepers are used in the field, the weak direction (i.e. perpendicular to grain), is subjected to longitudinal loads. The timber sleeper would have experienced damage prior to the spike damage under the longitudinal loads, unfavorably affecting the spike stress, which was also observed by Yu and Liu.[11] A comparative study was conducted to evaluate the spike stress in the GFRC and timber sleeper. Due to the anisotropy of timber sleeper, the spike stresses were quantified when loads were applied both parallel (//) and perpendicular (T) to the timber grain (Figure 11(b)). Material and strength parameters of a timber sleeper, calibrated with laboratory test data,[3] were incorporated into the FEM (Figure 11(a)) and were also run to provide a comparison of composite to timber.

Spike stress in the composite was 27% lower than a spike loaded in timber perpendicular to grain (T) with a longitudinal load of 8.9 kN (2000 lb.). These data indicate that a composite sleeper could take 27% more longitudinal load before exceeding the spike fatigue limit, relative to timber (T). However, the spike stress in the composite was 15% greater than a spike loaded in timber parallel to grain (//) when subjected to the lateral load of 8.9 kN (2000 lb.).

When the spike was loaded in the composite sleeper or parallel to grain in the timber sleeper, spike stress exhibited a nearly linear increase with load. In both cases, the corresponding compressive sleeper stress only slightly exceeded the compressive strengths of the composite or timber (//). The authors hypothesize that the spike in the timber (//) experienced less bending (i.e. and lower stress) at the same load because its MOE was 2.3 times greater than the composite. The spike stress and compressive stress of the timber sleeper (T) initially increased linearly with the applied longitudinal load. However, when the load exceeded 2.2 kN (500 lb.) there was a deviation with the composite because of the failure of the timber (T) grains.

Conclusions

To reduce the risk of spike fatigue failures that have led to multiple derailments and require manual walking inspections, the feasibility of using a composite sleeper as a mitigation method was investigated through a validated single-spike FEM. The FEM was validated using laboratory test data and was found to be capable of assessing the damage state of the spike and sleeper. The model results reveal how specific sleeper properties affect spike stress, which is applicable to all composite sleepers.

These quantified strength characteristics could be used to develop an engineered composite sleeper to reduce the risk of spike fatigue failures. The characterization of composite sleeper strength properties as presented can also be used to advance track system mechanistic-empirical analysis and design as proposed by Edwards et al.[35] The main findings are summarized as follows:

- Median composite sleeper compressive strength is:
  - 150% greater than timber perpendicular to grain and
  - 30% smaller than timber parallel to grain.
- Composite sleeper elastic modulus is:
  - 43% greater than timber perpendicular to grain and
  - 146% smaller than timber parallel to grain.
- The expected longitudinal loads can cause compressive strength failures in timber perpendicular-to-grain and some composite sleepers.
- The GFRC skin provides 70% greater MOE and 100% higher compressive strength than the core, decreasing the spike stress by 20% compared to the homogeneous composite sleeper.
- When the stress of the sleeper does not exceed the strength, as the skin MOE is increased the maximum spike stress would decrease by only 4%.
- When the stress of the sleeper exceeds the strength of the tie, as the compressive strength is increased the maximum spike stress would decrease by 12%.
- For the maximum expected load of 8.9 kN (2000 lb.), when sleeper compressive strength exceeds 34.5 MPa (5000 psi), the spike stress is below the fatigue limit and has little variation with additional compressive strength gains.

Acknowledgements

This research effort is funded by the Federal Railroad Administration (FRA), part of the United States Department of Transportation (US DOT) under Grant AF788 DOT FRA 693JJ612C000005. The material in this paper represents the position of the authors and not necessarily that of sponsors. J. Riley Edwards has been supported in part by the grants to the Illinois Rail Transportation and Engineering Center (RailTEC) from CN and Hanson Professional Services. Additional thanks to our industry partners: Norfolk Southern, CN, Union Pacific, CSX,

BNSF, Evertrak, Lewis Bolt & Nut Company, Vossloh North America, Progress Rail, and Pandrol USA, who provided materials, information, and expertise through the development of this research.

Declaration of conflicting interests

The author(s) declared no potential conflicts of interest with respect to the research, authorship, and/or publication of this article.

Funding

The author(s) disclosed receipt of the following financial support for the research, authorship, and/or publication of this article: This work was supported by the U.S. Department of Transportation grant (AF788 DOT FRA 693JJ612C000005)

ORCID iDs

Christian Khachaturian https://orcid.org/0000-0003-2821-7263
Marcus S. Dersch https://orcid.org/0000-0001-9262-3480
Shushu Liu https://orcid.org/0000-0001-5091-9304
J. Riley Edwards https://orcid.org/0000-0001-7112-0956

References

1. Khachaturian C, Dersch MS, Edwards JR, et al. Quantification of longitudinal fastener stiffness and the effect of fastening system loading demand. *Proc Inst Mech Eng F: J Rail Rapid Transit* 2021. DOI: 10.1177/09544097211030736.
2. Roadcap T, Kerchof B, Dersch MS, et al. Field experience and academic inquiry to understand mechanisms of spike and screw failures in railroad fastening systems. In: Proceedings of the 2019 AREMA Annual Conference with Railway Interchange. Minneapolis, MN: AREMA, 2019.
3. Dersch M, Roadcap T, Edwards JR, et al. Investigation into the effect of lateral and longitudinal loads on railroad spike stress magnitude and location using finite element analysis. *Eng Fail Anal* 2019; 104: 388–398. DOI: 10.1016/j.engfailanal.2019.06.009.
4. Dersch MS, Trizotto Silva M, Edwards JR, et al. Analytical method to estimate railroad spike fastener stress. *Res Rec J Transportation Res Board* 2020; 2674(11): 11, DOI: 10.1177/0361198120949259. pages. DOI:
5. Dersch MS, Trizotto M, Edwards JR, et al. Quantification of vertical, lateral, and longitudinal fastener demand in broken spike track: inputs to mechanistic-empirical design. *Proc Inst Mech Eng Part F: J Rail Rapid Transit* 2021. DOI: 10.1177/09544097211030736.
6. Dersch MS, Silva MT, Edwards JR, et al. Analytical nonlinear modeling of rail and fastener longitudinal response. *Transportation Res Rec J Transportation Res Board* 2022: 036119812110693. DOI: 10.1177/03611981211069350.
7. Liu S, Marquis B and Stuart C. Field validation of longitudinal rail load distribution model. In: Proceedings of the 2020 AREMA Conference, 2020. September 13-16, Virtual. St. Louis, Missouri, USA: American Society of Mechanical Engineers (ASME).
8. Hay WW. Chapter 25: fastenings and other track materials. In: *Railroad Engineering*. New York City, NY, USA: John Wiley & Sons, 1982, pp. 562–592.
9. Rippeth D, Kalousek J and Simmons J. A case study of the effect of lubrication and profile grinding on low rail roll-over derailments at CSX transportation. *Wear* 1996; 191(1–2): 252–255. DOI: 10.1016/0043-1648(95)06689-6.
10. Bergman R, Cai Z, Carll CG, et al. *Wood Handbook—Wood as an Engineering Material. General Technical Report FPL-GTR-190*. Madison, WI: U.S. Department of Agriculture, Forest Service, Forest Products Laboratory, 2010, p. 508.
11. Yu H and Liu S. *Proceedings of 2019 Joint Rail Conference*, 2019, p. V001T01A003.Finite element analysis of spike failure in elastic fastening systems for wood Ties. St. Louis, Missouri, USA: American Society of Mechanical Engineers (ASME).
12. Zakeri J and Rezvani F. Failures of railway concrete sleepers during service life. *Int J Construction Eng Manag* 2012; 1(1): 1∼5.
13. Ferdous W and Manalo A. Failures of mainline railway sleepers and suggested remedies – review of current practice. *Engineering Failure Analysis* 2014; 44: 17–35.
14. Ferdous W, Manalo A, AlAjarmeh O, Mohammed AA, Salih C, Yu P, Khotbehsara MM and Schubel P. Static behaviour of glass fiber reinforced novel composite sleepers for mainline railway track. *Engineering Structures* 2021; 229: 111627.
15. AREMA. *Manual for Railway Engineering*, 2018. Chapter 30 – Ties. Lanham, Maryland, USA: AREMA.
16. Gao Y and McHenry M. *Proceedings of 2019 Joint Rail Conference*, 2019, p. V001T01A017.Simulation of the thermal effects on engineered polymer composite ties. St. Louis, Missouri, USA: American Society of Mechanical Engineers (ASME).
17. McHenry M and Gao Y. Implementing improved composite tie design and testing guidelines into the AREMA manual for railway engineering. In: Proceedings of the 2018 AREMA Annual Conference. Chicago, IL, USA. Madison, WI: U.S. Department of Agriculture, Forest Service, Forest Products Laboratory, 2018.
18. Machado A. Polymeric sleepers—new development challenges. In: Proceedings of the 6th International Crosstie and Fastening Symposium. Champaign, IL. Urbana, Illinois, USA: University of Illinois, 24-25, 2022.
19. Gao Y and McHenry M. Development of a laboratory fatigue test for engineered polymer composite ties. In: Proceedings of the 2021 AREMA Annual Conference, Virtual, 2021. Lanham, Maryland, USA: AREMA.
20. Freudenstrain S. Laboratory testing of composite ties or composite bearers for turnouts. In: Proceedings of the 6th International Crosstie and Fastening Symposium. Champaign, IL. Urbana, Illinois, USA: University of Illinois, 24-25, 2022.
21. Axion. *Axion Safety Data Sheet (SDS)*, 2019. Zanesville, Ohio, USA: Axion.
22. Chow P, Reinschmidt A.J, Davis D.D, et al. *Proposed Strength Properties Tests for Wood Crossties: 3*, 1995. Vicksburg, Mississippi, USA: Railway Tie Association.
23. Lampo R, Nosker T, Gillespie B, et al. Performance and safety issues regarding the use of plastic composite crossties, 2001. Lanham, Maryland, USA: AREMA, https://citeseerx.ist.psu.edu/viewdoc/summary?doi=10.1.1.501.4040
24. Lavoie G.E.F & Co. Osb from wood strands and alternate fibers. United States Patent US2006/0148363 A1, Jul 6, 2006.
25. Maul E. Establishing the performance frontier for EPC ties in north american freight rail. In: Proceedings of the 6th

International Crosstie and Fastening Symposium. Champaign, IL. Urbana, Illinois, USA: University of Illinois, 24-25, 2022.
26. Lotfy I and Issa MA. Evaluation of the longitudinal restraint, uplift resistance, and long-term performance of high-density polyethylene crosstie rail support system using static and cyclic loading. *Proc Inst Mech Eng Part F: J Rail Rapid Transit* 2017; 231(8): 835–849.
27. TieTek. American tietek technical data: https://www.tietek.net/specsheets.asp (2017).
28. Tschernitz JL, Schaffer EL, Moody RC, et al. *Hardwood Press-Lam Crossties: Processing and Performance*. Madison, WI: U.S. Department of Agriculture, Forest Service, Forest Products Laboratory, 1979, p. 22. *Res. Paper FPL-313*.
29. Van Erp G and Mckay M. Recent Australian developments in fibre composite railway sleepers. *Electr J Struct Eng* 2013; 13: 62–66.
30. Koller G. FFU synthetic sleeper—projects in Europe. *Constr Build Mater* 2015; 92: 43–50.
31. Sengsri P, Ngamkhanong C, Melo M, et al. Damage detection in fiber-reinforced foamed urethane composite railway bearers using acoustic emissions. *Infrastruct* 2020; 5(6): 50.
32. Systèmes D. *Abaqus Example Problems Guide*, 2014. France: Dassault Systèmes, Vélizy-Villacoublay
33. Gao Y and LoPresti J. Technology Digest, *TD-20-004*. Pueblo, CO: Transportation Technology Center, Inc., 2020.Interim report broken spike remediation. Thousand Oaks, CA, USA: SAGE Publications, Inc.
34. Yu P, Manalo A, Ferdous W, et al. Screw lateral restraint behaviour of timber and polymeric based railway sleepers. *Eng Fail Anal* 2022; 139: 106514.
35. Edwards JR, Quirós-Orozco RJ, Bastos JC, et al. Vision for mechanistic-empirical railway track system and component analysis and design. *Transportation Res Rec J Transportation Res Board* 2021. 1–15. DOI: 10.1177/03611981211009881.

Author Biographies

Christian Khachaturian obtained his bachelor's and master's degree from the University of Illinois Urbana-Champaign. While he was pursuing his degree, he supported the tie and fastener project to evaluate mitigation methods for spike fatigue failure.

Marcus S Dersch, Ph.D., P.E. joined RailTEC in 2011 and is currently a Principal Research Engineer. He holds a B.S. (2009), M.S. (2010) and Ph.D (2022) in civil engineering from the University of Illinois Urbana-Champaign. While pursuing his degrees, he completed research in Railroad Engineering focusing on fouled railroad ballast performance and ballast performance improvement techniques. Marcus worked for Union Pacific Railroad as an engineering intern in 2008, obtained his Professional Engineer's License in 2015, and is the Chairman of AREMA Committee 30 (Ties). Marcus' current research interests are railway crosstie and fastener design and railroad ballast performance.

Shushu Liu, Ph.D., joined Volpe National Transportation Systems Center in 2018, and is currently a senior engineer. She obtained her Ph.D in civil engineering from Penn State with emphasis on railway geotechnics. Her research includes laboratory investigation, field instrumentation and numerical modeling of railroad track structure (ballast, tie and fastening system, etc.). She also provides support for modeling of railway passenger fuel tank and tank cars.

J Riley Edwards, Ph.D., P.E. is a Research Associate Professor in Railroad Engineering at the University of Illinois at Urbana-Champaign (Illinois). He obtained his bachelor's degree from Vanderbilt University and a Masters and Ph.D. in civil engineering from Illinois. Riley oversees research and advises graduate and undergraduate students concentrating in Railway Engineering. His research interests are railway track and component design and performance and span from rail transit to heavy axle load freight railroad applications.